Structurally optimized shells

FRANCISCA GIL-URETA, New York University
NICO PIETRONI, University of Technology Sydney
DENIS ZORIN, New York University

Shells, i.e., objects made of a thin layer of material following a surface, are among the most common structures in use. They are highly efficient, in terms of material required to maintain strength, but also prone to deformation and failure. We introduce an efficient method for reinforcing shells, that is, adding material to the shell to increase its resilience to external loads. Our goal is to produce a reinforcement structure of minimal weight. It has been demonstrated that optimal reinforcement structures may be qualitatively different, depending on external loads and surface shape. In some cases, it naturally consists of discrete protruding ribs; in other cases, a smooth shell thickness variation allows to save more material.

Most previously proposed solutions, starting from classical Michell trusses, are not able to handle a full range of shells (e.g., are restricted to self-supporting structures) or are unable to reproduce this range of behaviors, resulting in suboptimal structures.

We propose a new method that works for any input surface with any load configurations, taking into account both in-plane (tensile/compression) and out-of-plane (bending) forces. By using a more precise volume model, we are capable of producing optimized structures with the full range of qualitative behaviors. Our method includes new algorithms for determining the layout of reinforcement structure elements, and an efficient algorithm to optimize their shape, minimizing a non-linear non-convex functional at a fraction of the cost and with better optimality compared to standard solvers.

We demonstrate the optimization results for a variety of shapes, and the improvements it yields in the strength of 3D-printed objects.

CCS Concepts: • **Computing methodologies** → **Shape modeling**; *Mesh geometry models*; • **Mathematics of computing** → *Mathematical optimization*; • **Applied computing** → *Computer-aided design*.

1 INTRODUCTION

In structural design, shells are considered to be one of the most efficient structures because they can be simultaneously lightweight and robust. Shells are common in additive fabrication applications because using shells instead of solids reduces the cost of material and decreases the fabrication time.

An optimally-shaped shell can carry its load relying only on tensile/compression forces, with no bending involved, which is very efficient in terms of the required material. These types of shells are commonly found in architecture (domes). However, the shape of the shell may be determined by considerations other than its load-carrying properties. For example, the shape of the airplane is determined by its aerodynamics; the shape of the car body both by the aerodynamics and aesthetics; the top of a table or a shelf is

Fig. 1. Stages of our shell structure generation pipeline.

flat, as objects need to be placed on it; the artistic intent primarily determines the shape of a lamp or a statue.

Shell structures with shapes fixed by considerations other than loading are often reinforced by additional means, most commonly increasing thickness in critical areas or adding ribs (Fig. 2). Formally, a common optimization goal for a shell reinforcement structure is to *minimize the weight of the added material while keeping the maximal stress of the structure bounded*. The first ensures the structure remains lightweight, while the second prevents structural failure.

This problem has been well studied for two dimensions in the limit of low volumes. In 2D, the optimal layout forms a pattern of orthogonal lines (Hencky-Prandtl net) and, for a given layout, the minimum weight structure has all members fully stressed. These structures form, in the limit of low volumes, classical Michell structures and can be obtained by solving a convex optimization problem.

Fig. 2. Examples of shell structures showing variable thickness walls and ribs: (a) Gateway Arch monument; (b) beer bottle with standard thicknesses; (c) plastic shipping container; (d) plastic fork.

It is also well understood for pure bending problems for plates, i.e., the special case of flat shells with loads orthogonal to the surface; in this case, it also reduces to a different convex problem.

The situation is far more complex for the reinforcement of fixed curved shells embedded in three dimensions that we consider. For these shells, the weight-optimal structure may be locally either beam-like, forming *ribs* aligned with stress directions, or membrane-like, forming variable-thickness walls with no perforation [Sigmund et al. 2016]. The first case typically corresponds to bending-dominated regions while the second to areas dominated by in-plane forces. The optimal local structure is determined by the surface shape, the supports, and the loads.

In this general case, the problem is no longer convex and cannot be optimally solved either by methods that assume that result is only a variable thickness shell or by Michell-truss type methods.

In this paper, we propose a novel efficient computational method for constructing optimized reinforcement structures for shells naturally producing a full range of behaviors spanning the space between variable-thickness shell and rib-type reinforcement.

We partition the problem into three steps: (1) determine the field of (approximately) optimal stress directions; (2) construct the skeleton of the reinforcement structure that follows these directions, forming polygonal (predominantly) quad cells aligned with the field; (3) optimize how material is distributed inside the cells.

Contributions.

- For computing the field of optimal stress directions, we developed a generalization of Hencky-Prandtl nets which takes bending into account and can still be solved by minimizing a convex energy.
- For material distribution optimization, we use a low-parametric structure model for cells to efficiently optimize the distribution of the material. As the global optimization problem is *fundamentally non-convex* (we discuss the reasons on Section 3), to solve it we propose an efficient global/local method which shows stable and fast convergence behavior.

We demonstrate our approach by optimizing several 3D shapes. This evaluation shows our method can handle shells with arbitrary curvature, and successfully transitions between membrane- and

bending-dominated regions, obtaining the expected optimal substructures.

2 RELATED WORK

Our work builds on the ideas from classical structure design for 2D elasticity and plates, with the key ones originating the work of Michell [Michell 1904].

We complement these fundamental ideas with quadrangulation techniques which can be reinterpreted as a way to transition from an infinite continuum of field-aligned beams to its discretization. We use a variation of [Bommes et al. 2009], but any conforming, field-aligned method could be used (e.g., [Aigerman and Lipman 2015; Campen et al. 2015; Ebke et al. 2016; Kälberer et al. 2007; Myles et al. 2014a]). The optimization method for computing the optimal strain field can be viewed as a specialized cross-field optimization method. Similarly to the recently proposed method of [Knöppel et al. 2015] it has the advantage of being convex.

Shell Optimization. The closest works to ours are the recent works [Kilian et al. 2017] and [Li et al. 2017], with which we share a number of ideas. The former describes an elegant connection between curvature and Michell trusses and optimizes the surface shape so principal stress and curvature directions coincide. Only tensile forces are considered, and the volume approximation they use is valid for narrow beams (see Section 3). Similar to our work, [Li et al. 2017] keeps the shell surface fixed. This work considers a network of ribs, aligned with stress lines, and minimizes their volume; similarly to [Kilian et al. 2017], this work uses a narrow-beam approximation for the volume, and always produces a thin-beam structure. The cross-section shape of individual beams is optimized, which produces additional weight reduction. We discuss differences to these works in more detail in Section 8.

Our approach also shares similarity with [Groen and Sigmund 2017], which uses similar structures for constructing 2D optimized structures.

On the other extreme, [Zhao et al. 2017] considers optimization of variable shell thickness, while keeping the topology fixed, which is suboptimal for bending reinforcement. Our work aims to bridge the gap between these extremes.

The approach of [Pietroni et al. 2015] aligns a network of beams to an input stress field. Another recent related work, [Jiang et al. 2017] considers structures made out of beams with a small number of distinct cross-sections. Both methods are suitable for architectural design; instead, we focus on applications, like 3D printing, which allow greater flexibility of structures.

Structural Optimization. The literature on structural optimization is quite extensive, and there is no chance that we can do justice to all of it. The main types of approaches found in the literature include topology optimization methods (SIMP or ESO-based), analytic methods for optimal structures directly based on Michell-type theories, and methods based on shape derivatives (using an explicit or implicit evolving surface representation). Important books, which include reviews of many other works are [Rozvany 1976], [Allaire 2002], [Bendsøe and Sigmund 2004], as well as recent reviews, [Munk et al. 2015] and [Sigmund and Maute 2013].

The most prevalent methods in topology optimization of structures are based on SIMP-type methods (see [Bendsøe and Sigmund 2004] for a review), which relax the problem to optimizing a density over a domain, which is then converted to a structure by thresholding. This approach has many advantages, including simplicity of implementation [Sigmund 2001], connection to homogenization theory, flexibility in integrating functionals, and ease of scalable implementation ([Aage et al. 2015] and [Wu et al. 2016]). Nevertheless, the result will typically depend on initialization: for complex topology to emerge, the domain needs to be discretized using a fine grid. The parameters of the result (e.g., the sparsity of the structure, or minimal thickness) need to be controlled indirectly through algorithm parameters. Finally, the result is a voxelized structure, which then needs to be converted in some way to a form more suitable for manufacturing. In comparison, our method directly produces solutions based on a *globally optimal* field (in low-volume limit) and a beam skeleton for the optimized structure, which can be directly adjusted by the user in a variety of ways (e.g., converted to a spline-based CAD model if desired). We compare in more detail in Section 8.

Ground structure methods are among the oldest methods for optimizing topology of truss/beam structures. These methods start with a structure consisting of a large number of redundant beams and optimize it to determine the cross-sections, which automatically eliminates some of the beams. Recent examples of applying these type of methods include [Sokół 2011; Zegard and Paulino 2014, 2015]. Compared to our approach, ground structure methods have to restrict the directions of beams to a small set, which affects both optimality and flexibility of the design. The larger the initial set of beams, the closer they may approximate the optimal result. In computer graphics, the ground structure method was used early in [Smith et al. 2002] for truss structure design. [Panetta et al. 2015] used a version of a ground structure method to obtain initial topologies for computing microstructures with prescribed material properties, followed by shape optimization.

To a great extent, our work was inspired by the beautiful structures explored in the literature on analytic or semi-analytic structure design, e.g. [Rozvany 2012], which includes many examples of exact problem solutions, such as Hencky-Prandtl nets. Our goal is to use this type of ideas in the general setting of surface domains, taking advantage of the optimality criteria and insights into the structure of the solutions. A concise exposition of the theory underlying Michell-type optimal layouts can be found in [Strang and Kohn 1983]. We note that the application of Michell-type structures in 3D is only appropriate for certain problem settings: e.g., with no lower-bound constraints on shell thickness, variable thickness shells are likely to emerge as a solution [Sigmund et al. 2016].

Shape-derivative based optimization techniques (e.g., [Allaire and Jouve 2008]) can obtain very good results when one needs to improve an existing design, by evolving the shape to a local minimum. However, while level-set methods of this type allow for topology changes, the result does vary considerably depending on the starting point. In contrast, our goal is to obtain a starting point that is close to the global optimum, as long as the desired structure has a relatively low volume.

Digital fabrication. The works closest to ours in this domain are [Li and Chen 2010], [Tam et al. 2015], and [Tam 2015]. These methods are based on constructing structures from stress lines on surfaces which, while different from the optimal fields we compute, are often a close approximation. The overall pipeline of the method of [Li and Chen 2010] is similar to ours: they start with a field, and construct trusses following the field by tracing lines from supports to loads. The method is limited to two dimensions and demonstrated only for relatively simple structures.

[Tam et al. 2015] uses FDM to add material directly along the principal stress lines, on 2.5D surfaces. The main problems they solve are stress line generation and selection. They minimize strain energy subject to a maximal total print length (i.e max material) and a consistent maximum spacing between lines.

Applying topology optimization (SIMP and ground structure methods) to 3D printing applications is discussed in [Zegard and Paulino 2016].

3 MOTIVATING EXAMPLES

To motivate our method, we start with simple examples of qualitatively different behavior of optimized structures.

The two key behaviors of shell-like optimal structures, observed in special-case analytic solutions and topology optimization (cf. [Sigmund et al. 2016]), are the formation of discrete narrow *ribs* protruding from the surface in bending-dominated cases (most forces are perpendicular to the surface), and relatively smooth variation in shell thickness in the pure tensile/compression case (in-plane forces), as shown in Figure 3.
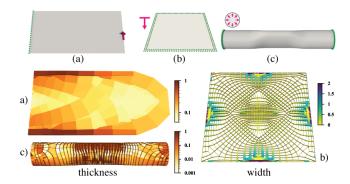

Fig. 3. (a) optimal structure for a standard cantilever test case with variable thickness, cf. [Sigmund et al. 2016] (b) bending plate optimization, resulting in a rib structure qualitatively consistent with analytical results; (c) an optimized pipe structure exhibiting a mix of behaviors.

These behaviors are *not* observed in the simplified models of beam networks approximating a surface: beams in a typical network do not expand in the direction parallel to the surface, to merge into a variable-thickness shell optimal in such cases. It turns out that this is due to the qualitatively inaccurate volume computation with the volume of the beam network approximated by the sum of individual beam volumes. We now consider two simple examples showing why this is the case.
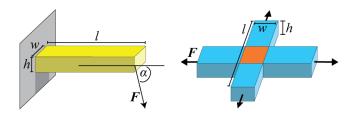
Fig. 4. Left: beam loading and parameters; Right: surface approximated by two intersecting beams loaded in plane.

First, we consider optimization of a single horizontal beam of width w and height h, clamped at one end, and loaded at the other, at an angle α to the beam direction (Figure 4, left). This example clarifies optimal behavior when there is stress in only one direction, both for bending ($\alpha = \pi/2$) and tension ($\alpha = 0$). The second example involves two intersecting beams (Figure 4, right). It is a simple model for a piece of a surface with there is stress in two directions.

For a single beam, the force along the beam is proportional to the cross-section wh. The force *perpendicular* to the beam (bending) is proportional to wh^3. The total force is proportional to $\cos\alpha\, wh/l + \sin\alpha\, wh^3/l^3$, where l is the beam length, and $\cos\alpha$ and $\sin\alpha$ are due to projection to the direction of F. For simplicity, assume the proportionality constant to be 1. We optimize the beam volume whl, keeping the force balance constant: $\cos\alpha\, w(h/l) + \sin\alpha\, w(h^3/l^3) = F$. Eliminating w, yields unconstrained minimization of $V = Fl^2/(\cos\alpha + y^2 \sin\alpha)$, with $y = h/l$. Clearly, the solution is to maximize the relative thickness $y = h/l$, if $\sin\alpha \neq 0$: increasing thickness has a higher payoff as forces grow as h^3 vs. only h for width. However, in the case of a vertical beam, $\alpha = 0$; the constraint takes the form $wy = F$, i.e., the volume value is fixed and the choice of y makes no difference. We conclude that the solution can be always taken to be the "thick but narrow" beams (we refer to them as *ribs*), with maximal possible h.

The situation is more complicated for surfaces. In the second example, we approximate the surface locally by beams aligned with the perpendicular stress directions (see figure 4 right). For simplicity, we assume the forces, widths w, lengths l and thicknesses h to be the same for both beams. If we view the intersecting beams individually and approximate the total volume as $V = 2whl = 2wyl^2$, then the reasoning above applies to each beam: for $\alpha = 0$, only the cross-section matters, but even a small bending component will prioritize maximal h solutions, so both beams will be thick and narrow; for in-plane forces F, we get $wy = F$ and the optimal volume $V = 2Fl^2$ no matter which w we use.

Considering beams in separation ignores the fact that *the intersection area of the beams is counted twice*: this part of material is performing "double work", supporting loads in two directions along two beams. The correct combined volume of two beams is given by

$$V'(w, y) = 2wyl^2 - w^2yl,$$

assuming the same beam width and thickness for both. For in-plane forces, as before, we have the constraint $wy = F$ for constant F. The functional V' can be expressed then as $V'(w) = Fl(2l - w)$, by eliminating y. From the expression it is clear that one would want to maximize the *width* in this case as opposed to *thickness*. The optimal

volume for max thickness $w = l$ is Cl^2. In comparison, if we use large thickness $y = C/w$, then optimal $w \approx \epsilon$ is close to zero, and the volume $V'(\epsilon)$ is close to $2Cl^2$, two times higher than optimal $V'(l)$.

In the case of two intersecting beams with an out-of-plane load in addition to in-plane, requiring a combination of a tensile and bending force to support, there is an optimal trade-off between w and h minimizing the volume, as long as loading cannot be supported by pure bending forces.

If we further impose constraints on maximal and minimal surface thickness, even in tensile-dominated areas, beams would form, because the optimal solid shell there would be too thin. A general optimization method should be able to smooth between grillage-like structures for bending dominated areas and "thin and wide" structures for the rest of the surface.

We conclude, from these examples, that to reinforce a shell in a manner close to optimal for arbitrary loads and shell shape, both solid variable-thickness and rib-like structures may be required in different areas of the surface, and for these to emerge, in a beam-based optimization problem, a non-convex volume function accounting for beam intersection areas has to be used.

4 PROBLEM FORMULATION

We start with a description of the discretization of variable-thickness perforated surface shell structure that we use, and the optimization problem we aim to solve.

4.1 Perforated variable thickness shells

Our input is a shell M of an initial thickness h_0 (constant per triangle) represented by a triangle mesh, with a vector of external forces f applied to its vertices, and a set of fixed vertices (supports).

We aim to compute an optimized shape which we call a *perforated shell of variable thickness* M^p. M^p consists of (a) a partition $\mathcal{P}$ of the input surface into polygonal faces (typically quads), corresponding to 3D *cells*, and (b) an extruded shape for each cell, consisting of *blocks* as described below.

Given an approximate user target for cell size, our goal is to optimize the edge orientation of the cell boundaries, and thicknesses and width of blocks forming each cell to minimize the weight, while maintaining an upper bound on stresses (calculated using a beam model). M^p can be viewed as the reinforcement structure for M.

Cell geometry parametrization. For each edge of a face of M^p we introduce two parameters, *width* w_i and *thickness* h_i. With each edge, we associate a hexahedron (block) constructed by creating a strip inside the face at distance w_i from the edge and extrude the resulting trapezoid along the triangle normal (See Figure 5). While this geometry may result in gaps between adjacent cells, this has no mechanical implications as we treat each block as anchored to edge vertices. We model each side of the cell as a beam including tension/compression and bending forces. While this is a very coarse approximation of the shape, it allows us to obtain an approximation of the solution robustly and quickly. This results can be further refined by shape optimization methods (e.g. [Panetta et al. 2015]).
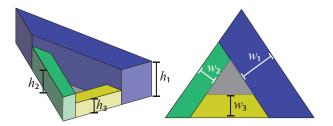
Fig. 5. Geometric parametrization of triangular cell. Left: perspective view; Right: top view.

Fig. 6. Beam bending discretization.

Volume discretization. To simplify our problem, we split all polygonal cells into triangular subcells. We refer to the additional edges inserted in this way as *diagonals*. We treat these in a special way in the optimization, and in the end ensure that the triangular cells can be merged back into the original polygonal cell (Section 7).

We consider triangular cells with sides l_i, $i = 1, 2, 3$, and blocks with rectangular cross-sections of width w_i and thickness h_i along the edge l_i (Figure 5). The simplest approximation of the volume which is typically used in low-volume truss models, when applied to our system would yield simply $\sum_i w_i h_i l_i$. However, as discussed in Section 3 this approximation of the volume results in highly sub-optimal results for shells regions dominated by tensile forces.

A more precise approximation is the volume of the extrusion of 3 trapezoidal regions by different heights. Denote $y_i = w_i/a_i$, where a_i is the height of the triangle with base on side l_i, $A = \frac{1}{2} a_i l_i$ for any i is the area of the triangle. Let (i, j, k) be the permutation of $(1, 2, 3)$ for which $h_i \geq h_j \geq h_k$, the volume is given by the following simple expression:

$$V(w, h) = A \left((2 - y_i) y_i h_i + (2 - 2y_i - y_j) y_j h_j \right.$$
$$\left. + (2 - 2y_i - 2y_j - y_k) y_k h_k \right) \tag{1}$$

This volume can be written as $V(w, h) = \max_{(i,j,k)} V_{ijk}(w, h)$, where $V_{ijk}(w, h)$ is given by (1) for arbitrary permutation (i, j, k). This expression for the volume is useful for the optimization method in Section 7.

The out-of-plane heights can be constrained not to exceed a user-defined value h_{max}, and the normalized widths y_i are constrained so that the trapezoidal areas do not overlap:

$$y_1 + y_2 + y_3 \leq 1, \quad y_i \geq 0, \quad 0 \leq h_i \leq h_{max}, \text{for } i = 1, 2, 3 \tag{2}$$

4.2 Elastic deformation discretization

We model the perforated shell structure as a *beam network:* for each interior edge, there are two beams, corresponding to the blocks of incident cells along the edge.

Notation. The beam network consists of a set of beams $\mathcal{E}$ that are joined together at nodes. For a node i, $N(i)$ is the set of indices of nodes connected to it, and the vector $\mathbf{e}_{ij}$ connecting nodes i and j corresponds to the edge e_{ij}. For each edge, $\hat{\mathbf{e}}_{ij}$ denotes the unit vector along $\mathbf{e}_{ij}$. The edge e_{ij} has length ℓ_{ij}. We assume that all cells are made of uniform material with E as Young modulus. We use $\sigma[ij]$ and $\varepsilon[ij]$ notation for the one-dimensional (tensile or bending) stresses and strains of beam connecting vertices $i j$ in a given cell.
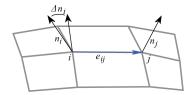
Beam linear elasticity discretization. The tensile strain along each beam is the scalar $\varepsilon^t[ij] = (\mathbf{u}_j - \mathbf{u}_i) \cdot \hat{\mathbf{e}}_{ij}/l_{ij}$, same for both blocks at the edge e_{ij} where $\mathbf{u}_i$ is the displacement of a vertex i. It is related to the stress by $\varepsilon^t[ij] = \sigma^t[ij]/E$.

For our problem, bending discretization is critical. We use a pure displacement-based beam bending approximation, but a more standard beam element could be used. Our beams are *clamped* to a freely rotating plane at each vertex, i.e., preserve the angle between the beam and the (freely moving) normal to that plane. We use a simple discrete beam model for bending: we neglect the torsion and shear and define the bending strain, i.e., the change in the curvature of a beam e_{ij} as

$$\varepsilon^b[ij] = \hat{\mathbf{e}}_{ij}^T (\Delta \hat{\mathbf{n}}_j - \Delta \hat{\mathbf{n}}_i)/l_{ij}, \tag{3}$$

where $\hat{\mathbf{n}}_i$ and $\hat{\mathbf{n}}_j$ are normals meeting at nodes i and j (Figure 6), and $\Delta \hat{\mathbf{n}}$ denotes linearized change of the normal. The normal change, in turn, is expressed in terms of the displacements $u_{i\ell}$, $\ell \in N(i)$ of the incident vertices.

This leads to the expression for a scalar bending strain on beams:

$$\epsilon[ij]^b = (D_{ij}^b)^T u \tag{4}$$

with the expressions for D_{ij}^b given in the Appendix.

At a distance z from the middle surface of a beam, the strain is given by $\epsilon^t + z\epsilon^b$, where we omit the beam index. Based on the standard Bernoulli beam assumptions after integration over $z \in [-h/2, h/2]$ the total beam energy can be expressed as

$$\frac{1}{2} (wlhu^T (D^t)(D^t)^T u + \frac{1}{6} wh^3 l u^T (D^b)(D^b)^T u),$$

which leads to the following expression for the stiffness matrix of the beam system:

$$K = wlh(D^t)(D^t)^T + \frac{1}{6} wh^3 l(D^b)(D^b)^T \tag{5}$$

Given the expression for strain $\epsilon^t + z\epsilon^b$, clearly both strain and stress are maximal on one of the surfaces, i.e., for $z = h$ for a given beam. This leads to the following stress constraint:

$$|(D_{ij}^t + h_{ij} D_{ij}^b)^T u| < \sigma_0 \tag{6}$$

Optimization problem. We use index c for triangular cells. Let w is the vector of width parameters of all cells, y is the vector of corresponding normalized widths w_i/a_i, h is the vector of all thickness parameters, H the diagonal matrix with thicknesses on the diagonal, and u and f are displacements and forces respectively. Let $\mathbf{1}$ be the vector of all ones.

We now formulate our general optimization problem:

$$\min_{h, y, \mathcal{P}} \sum_{c \in cells} V(h_c, y_c) \quad \text{s.t.} K(h, y)u = f,$$

$$|(D^t \pm D^b H)^T u| \leq \sigma_0 \mathbf{1}, \quad 0 \leq h \leq h_{max}, \quad y \geq 0, \tag{7}$$

$$y_1^c + y_2^c + y_3^c \leq 1, \text{ for all cells } c, i = 1, 2, 3$$

where the absolute value in the stress constraint is taken element-wise, $\mathbf{1}$ denotes a vector of ones, and the minimum is taken over all partitions $\mathcal{P}$ of M into triangulated cells. Additionally, we enforce the same thickness on two sides of all cell diagonals.

As optimization over all possible partitions into cells is an intractable problem combining combinatorial and continuous aspects, we use an heuristics to fix the partition first, using *beam continuum approximation* (Section 6). Once E is fixed, we optimize with respect to w and h only.

While the above formula volume differs only by a seemingly simple quadratic term from the simplest approximation, this completely changes the behavior of the problems, and, in particular, the behavior of the solvers. The problem no longer reduces to convex by a change of variables as it is the case for the simplest formula (cf., e.g., [Hemp 1973]), and a different type of solvers need to be applied. In our experiments, commonly used general purpose non-convex solvers converge very slowly and often fail to make progress. Our solution is described in Section 7.

5 OVERVIEW OF THE APPROACH

Our pipeline for solving the optimization problem consists of the following steps.

(1) **Field optimization.** Compute a per-triangle cross-field on surface using stress-based optimization (Section 6). This field corresponds to an idealized system of densely spaced thin beams (*beam continuum*) with directions chosen to minimize weight. The problem is formulated in terms of displacements and the desired cross-field is obtained from the symmetric strain tensors. This requires solving a convex optimization problem with inequality constraints.

(2) **Quadrangulation.** Create a quad-dominant mesh aligned to this cross-field with a user-controlled spacing of edges. This step is done using a version of mixed-integer quadrangulation [Bommes et al. 2009], although any quad layout method with field alignment can be used (Section 7). The faces of the mesh will correspond to the *cells* of the perforated shell M^p.

(3) **Cell optimization.** Optimize shape parameters of the cells (Section 7). This step has a maximal impact on the final outcome. We introduce a substructure for each cell, with a small number of control parameters defining its shape (widths w and thicknesses h of rectangular beams along each side). We derive the optimal material distribution by efficiently solving a nonlinear, non-convex problem minimizing the total volume of all cells with respect to w and h, while keeping stresses below a user-defined maximum. To make the problem tractable we defined an efficient local-global optimization method.

(4) **Final geometry construction.** Finally, we derive the final geometry of M^p according to optimized widths and thickness. We obtain a triangle mesh by performing a sequence of boolean operations between meshes representing the beams. The final watertight and manifold mesh can be directly used for 3D printing or decomposed into cells for FEM analysis.

In the following sections, we describe the details of the steps of the pipeline.

6 WEIGHT-MINIMIZING FIELD OPTIMIZATION

In this section, we describe our method for constructing a field of directions on the surface approximating optimal directions for weight minimization with bounded stress. The cells in our construction will be aligned with these directions.

The key idea is to solve a version of the beam weight minimization we assume that there is a *continuum* of infinitely thin infinitely close beams in two orthogonal directions forming the surface. The density of the beams and their orientations are the optimization variables. The idea of using this type of continua goes back to [Michell 1904].

In the simplest case of planar elasticity (which is largely equivalent to the case of a fixed thickness shell in this case) the problem was extensively studied and was shown to reduce to a convex problem. We first describe this classical theory (Michell continua) and then extend it to the case of shells with bending forces (Section 6).

6.1 Michell continua

Here, we briefly review the classical solution, following [Strang and Kohn 1983]. The best directions are known to be the principal stress directions of the *optimized* structure. (These are *not* the same as the stress direction on the original shell, although these fields are often close.)

The force balance for a plate or a shell with no bending is given by the standard equations in terms of in-plane stress tensor σ, strain ε, possibly varying elasticity tensor $E(\mathbf{p})$, and external force density $\mathbf{f}$:

$$\text{div}\sigma = \mathbf{f}, \ \sigma = E(\mathbf{p}) : \varepsilon; \ \varepsilon = \frac{1}{2}(\nabla \mathbf{u} + \nabla^T \mathbf{u}). \tag{8}$$

where $A : B = \sum A_{ijkl} B_{kl}$ for a 4-tensor and a 2-tensor.

A Michell continuum is an idealization of a beam network, characterized, at every point, by beam densities ρ_1 and ρ_2 in two directions, in other words, how many beams cross a unit-length segment along one of the coordinate directions. In the limit of small thicknesses, the total fraction of a small area covered by trusses at a point p is $\rho_1(p) + \rho_2(p)$. The total volume of the trusses in the continuum can be defined as $\int_\Omega \rho_1 + \rho_2 dA$. Note that this approximation of area covered by trusses suffers from the same flaw pointed out in Section 3.

The optimal trusses have to be oriented along stress directions, and be critically stressed, i.e., all (non-averaged) stresses on the trusses are equal to maximal stress σ_0. This leads to the relationship between ρ_i and corresponding averaged principal stress: $\lambda_i(\sigma) = \rho_i \sigma_0$, $i = 1, 2$, where $\lambda_i(\cdot)$ denotes the i-th singular value.

Then, we obtain the following optimization problem for the volume, formulated entirely in terms of stresses.

$$\text{minimize} \int_{\Omega} |\lambda_1(\sigma)| + |\lambda_2(\sigma)| dA, \text{ subject to } \text{div}\sigma = \mathbf{f}. \quad (9)$$

where σ_i are singular values of the stress tensor. This problem is known to be *convex* [Strang and Kohn 1983] (although it is more difficult than the linear programming formulation for a truss network). Note that principal stress directions are not fixed and are determined by the optimization. We use these directions as the field for orienting beams in M_p.

The problem (9) has a simple dual (see appendix) of the form

$$\text{maximize} \int_{\Omega} \mathbf{f}^T \mathbf{u} dA \text{ subject to } |\lambda_i(\varepsilon)| \leq \varepsilon_0, i = 1, 2. \quad (10)$$

Where ε is the strain of the optimal solution. The dual problem is significantly easier to deal with in the case of continua.

We note that here we neglect the overlap volume of trusses discussed in Section 3; while it could be included as $-\rho_1\rho_2$ term, this would immediately make the problem non-convex, and the benefit of more precise field optimization in terms of volume reduction is minor (Section 8).

6.2 Continuum optimization with bending

Next we generalize problem (10) to include bending forces.

If the thickness of the shell remains fixed, one can add bending to the functional with relative ease without changing convexity of the problem. We set the shell thickness in this case to half of the maximal allowable thickness; while the resulting field is suboptimal, as we show experimentally in Section 8, inaccuracy in the beam direction has less effect on the overall weight reduction, compared to width/thickness optimization of beams.

We make the standard assumption of planar stress for the shell, i.e., no stresses are active in the direction perpendicular to the shell surface. The strain at a distance z from the midline of the shell is given by

$$\varepsilon(z) = \varepsilon^t + z\varepsilon^b,$$

where ε^b is the *bending strain* tensor, equal to the linearization of the change in the shape operator $\nabla\hat{\mathbf{n}}$ (Figure 8)

Consistently with the Michell continuum, we seek to minimize the total weight of a beam continuum, bounding the stress everywhere by σ_0. We observe that the eigenvalues of a 2×2 symmetric matrix A using the already mentioned substitutions $a = (A_{11} + A_{22})/2$,

Fig. 8. Vertical strain distribution in a shell.

$b = (A_{11} - A_{22})/2$, $c = A_{12}$, are of the form $a \pm \sqrt{b^2 + c^2}$. Note that these are respectively convex and concave functions of the argument, and, therefore, reach their maxima (respectively minima) on the boundary of the shell, for $z = \pm h$. For this reason, it is sufficient to bound eigenvalues of stress (or strain) only for $z = h$ and $z = -h$, to guarantee the bounds elsewhere.

In the case of bending, the dual problem formulated in terms of displacements has a simpler form relative to the primal problem:

$$\text{maximize} \int_{\Omega} \mathbf{f}^T \mathbf{u} dA \text{ subject to } |\lambda_i(\varepsilon^t \pm \frac{h}{2}\varepsilon^b)| \leq \varepsilon_0, i = 1, 2. \quad (11)$$

Note that now there are two sets of constraints, corresponding to two surfaces of the shell.

The strain tensors $\varepsilon(h/2)$ and $\varepsilon(-h/2)$ can be interpreted as defining cross-fields on the surface. We use the angular average of these fields to align the cells. Finally, we describe a discretization of this convex problem, and how to use the resulting field to build a mesh.

6.3 Discretization and field smoothing

As a first step, we solve a discrete version of the problem (11), which yields displacements $\mathbf{u}$ at vertices. From these displacements, we compute the per-triangle strain field eigenvectors, forming a cross-field on the surface, i.e., an assignment of 4 unit vectors, aligned with perpendicular principal strain directions, to each triangle.

This field is only partially defined: we discuss the properties of the solution that allow us to identify areas of the mesh where the directions of the field can be used. In the areas where the field is not defined or is numerically unstable, the beam orientation is not relevant (in the limit of infinite beam density), and we extend the field smoothly. We use a cross-field construction procedure of [Bommes et al. 2009] to complete the field to the whole surface, identifying, along the way, the singularities of the field.

Discretization of the optimization problem. The optimization problem (11) has a relatively simple discretization that can be readily plugged in into a cone program solver. e.g., [ApS 2015].

We assume that the surface is given as triangle mesh, $M = (V, E, F)$, and the same notation is used for edge vectors and vertices as we used for beam networks.

The variables in the problem are displacements, which we discretize using standard piecewise-linear functions on the surface, with the vector of unknowns u (we use non-bold letters for high-dimensional vectors including all components of corresponding three-dimensional quantities).

The two quantities that need to be discretized are tensile and bending strains; we define these per triangle.
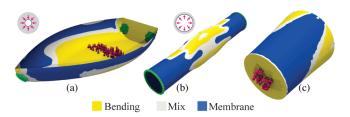

Fig. 7. Loaded shells dominated by bending and tensile forces, and a mix of these. Support nodes are highlighted in green while loads are shown in red. Loads on (a) and (b) include, respectively, external and internal pressure.
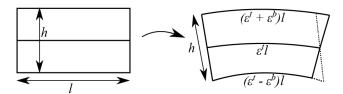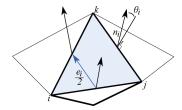
Fig. 9. Discretization of the bending field.

If $\mathbf{e}_{ij}$ are the vectors along triangle edges, for a triangle T, we have the following expression for the strain, computed as $\frac{1}{2}(\nabla u + \nabla^T u)$:

$$\varepsilon_T^t = \frac{1}{4A_T}\left(\sum_{i=1,2,3} \mathbf{e}_{jk}^{\perp} \mathbf{u}_i^T + \mathbf{u}\mathbf{e}_{jk}^T\right) \tag{12}$$

where A_T is the triangle area, j is the vertex after i in CCW order, k is before i, and $\mathbf{e}_{jk}^{\perp}$ is the vector in the triangle plane perpendicular to the side.

If by abuse of notation, we use ϵ_T^t to denote the vector of three distinct components of the strain tensor, we can write the expression in the form $B_T^t u$, where u is the vector of all displacement degrees of freedom.

To discretize the bending strain, we use the triangle-based approximation of the shape operator, following the overall idea in [Oñate et al. 1994] and [Grinspun et al. 2006], using vertices of the edge-adjacent triangles to compute the changes of the average normals at edge midpoints, and computing the gradient of the normal using the formulas (12).

This leads to the following expressions for the bending strain on triangles, in which we neglect the triangle deformation: in the deformation modes for which the bending strain is high (i.e., if the curvature changes a lot, in-plane deformations are small). We use the following formula [Grinspun et al. 2006], Figure 9:

$$\epsilon_T^b = \sum_{i=1,2,3} \frac{\theta_i}{2Al_i}\mathbf{e}_i^{\perp}(\mathbf{e}_i^{\perp})^T \tag{13}$$

where θ_i are linearized *changes* in the angles between normals of adjacent triangles.

Similarly to ε^t, we can write $\varepsilon^b = B^b u$. Then the discrete problem takes the form

maximize $f^T u$ subject to, for all T, $|\lambda_i(B_T^t \pm hB_T^b)u)| \le \varepsilon_0, i = 1, 2$. (14)

where f, similarly to the beam case, denotes the vector of per-vertex forces, and u is the vector of all vertex displacements. We use eigenvalue formulas defined for (18) to convert the problem to a convex cone problem, which we solve using the MOSEK solver [ApS 2015].

Detecting field zones. While the output of the previous step defines a tensor for each triangle, not all of these are meaningful. In some cases (if the triangle is not deformed at all, or deformed negligibly) the strain is zero. More generally, some points may have isotropic strains of the form kI, where k is a nonzero constant, for which all vectors are eigenvectors, so the cross-field is not defined uniquely

$\bullet\lambda_1 = -\lambda_2 = \pm\varepsilon_0$ $\bullet\lambda_1 = \lambda_2 = \pm\varepsilon_0$ $\circ|\lambda_2| < |\lambda_1| = \varepsilon_0$ $\circ|\lambda_1|, |\lambda_2| < \varepsilon_0$
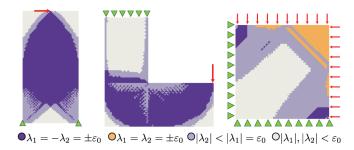
Fig. 10. Zones of an optimal strain field. The crossfield directions are well-defined only for regions 1, 3 (purple).

on this triangle. For general fields, such points are usually isolated. However, for the fields corresponding to the solution of the problem we are considering, the situation is different. There are three possible regimes (see, e.g., [Strang and Kohn 1983]). Specifically, the possibilities include

(1) $|\lambda_1(\varepsilon)| = |\lambda_2(\varepsilon)| = \varepsilon_0$, $\lambda_1(\varepsilon)\lambda_2(\varepsilon) = -\varepsilon_0^2$, principal strains are critical and have opposite directions; this corresponds to well-defined two orthogonal beam families;

(2) $|\lambda_1(\varepsilon)| = |\lambda_2(\varepsilon)| = \varepsilon_0$, $\lambda_1(\varepsilon)\lambda_2(\varepsilon) = \varepsilon_0^2$, principal stresses are critical and have the same direction; in this case, beams are not defined;

(3) $|\lambda_1(\varepsilon)| = \varepsilon_0$, $|\lambda_2(\varepsilon)| < \varepsilon_0$; this corresponds to a single family of beams;

(4) $|\lambda_1(\varepsilon)| < \varepsilon_0$, $|\lambda_2(\varepsilon)| < \varepsilon_0$: in this case, stresses (which are dual variables to the inequality constraints) are both zero, which means there are no beams in this area.

In cases 1 and 3, the crossfield directions are well-defined (purple zones on Fig. 10). In cases 2 and 4 these are either not defined or are not relevant, due to the absence of structure. For this reason, for our construction, we use only regions 1, and 3, which we detect by requiring at least one eigenvalue to be close to ε_0, and the difference of eigenvalues to be more than a constant.

We call the resulting field *salient*. The situation is essentially identical to the cross-fields used for constructing quadrangulations: typically, a field aligned with curvature directions is used as a starting point, and only in areas where the difference of two principal curvatures is high.

Completing the field. To complete the field on the whole surface, which is needed for a complete structure, we use cross-field constrained optimization procedure of [Bommes et al. 2009]. In this algorithm, the cross-field is encoded by a per-triangle angle, with respect to a reference direction β_i in each triangle. The angles on salient triangles are fixed. On the remaining triangles, these are found by a greedy solve of a mixed-integer problem minimizing the energy

$$E = \sum_{\text{edges}(ij)} (\beta_i - \beta_j + k_{ij}\frac{\pi}{2} + \kappa_{ij})^2$$

where the summation is over all dual edges connecting triangles i and j, κ_{ij} is the angle between reference directions in triangles, and

k_{ij} is an integer unknown accounting for the fact that cross-field values represented by angles $\beta + k\pi/2$ are the same.

In the resulting field, defined by the angles β_i for all triangles, and integers k_{ij} for all edges, one can easily compute per-vertex field index and identify field singularities, which become irregular (valence different from 4) vertices of the quad mesh at the next step. We refer to [Bommes et al. 2009] for details of the index computation.

6.4 Construction of the quad-dominant network

In general, there may be no optimal beam spacing (in the low-volume limit, the finer the structure, the lower the optimal volume can be for a given stress). For this reason, the beam spacing is defined by a user-specified parameter H. The most direct approach for constructing a quad mesh aligned with a field would be to trace it. However, while it was shown [Myles et al. 2014b; Ray and Sokolov 2014] that this approach can be implemented robustly, in general it requires T-joints (i.e. beams joining other beams in the middle), and it is in general hard to ensure uniform spacing over the whole mesh. We choose a more conservative approach based on constructing a conforming quadrangulation, without T-joints, using a version of the mixed-integer quadrangulation algorithm [Bommes et al. 2009] at this step.

While the method does not guarantee perfect alignment of the parametric lines to the input field, it minimizes the deviation in least-squares sense. We refer to [Bommes et al. 2009] for further details.

7 OPTIMIZING CELL GEOMETRY

Given an input quad-dominant mesh, split into triangles, we aim at deriving the optimal width and thickness for each edge. As we previously stated, to derive an optimal structure it is important the edges follow the directions we derived in the field optimization step. While our material distribution optimization method works for any mesh, the further the edges deviate from their optimum directions the greater would be the total weight.

7.1 Optimization algorithm

We introduce a domain-decomposition-style algorithm for solving the problem (7). We observe that in the optimization problem (7), all constraints except $Ku = f$ are localized, i.e., each constraint uses variables related to one cell. Moreover, the functional itself is a sum of local volume terms $V^c(w^c, h^c)$. $Ku = f$ expresses the equation of force balance, i.e., that the sum of beam forces at each node is equal to the external force at this node. Our approach is to fix individual beam forces to their values for current values of geometry parameters w and h, and then solve for an update to w and h as a set of local volume-minimization problems with variables w^c, h^c, replacing the global constraint $Ku = f$ with local constraints requiring that individual beam forces remain the same.

We start with an outline and then elaborate on how the local step optimization problems are solved.

Initially, we assign sufficiently high values to w and h, to ensure that max stress constraints are satisfied.

- **Global step.** The global step is just the standard solve of the elastic equilibrium problem, for fixed cell parameters: *Solve $Ku = f$, for fixed K defined by w and h. Compute beam forces as described below.*
- **Local step.** The local step is the key part of our algorithm. Recall that an important feature of optimal structures is that they are *critically stressed* i.e., the maximal stress on any element is equal to the maximum possible σ_0. The reasons for this are straightforward: if a stress on an element is below zero, one is free to remove some material, increasing the stress on the remaining part, and decreasing the weight.

  This motivates our approach. For the local step, we keep the displacements computed at the global step fixed and solve for widths and thicknesses, that would result in maximal stresses on blocks reaching the critical value σ_0 for given displacements. Each system has 6 unknowns, with 3 constraints on stresses.

Block forces. To formulate our local algorithm, we introduce *block forces*, for individual blocks of each cell; we determine w^c and h^c for each cell by minimizing the cell volume, while keeping the block *critically stressed* i.e., with maximal stress σ_0 and block forces constant.

Let K^{loc} be the element stiffness matrix corresponding to a block B. The vector of forces corresponding to a beam is the vector $\nabla_u E^{loc}$, i.e. the derivative of the block energy $E^{loc} = \frac{1}{2}u^T K^{loc} u$ with respect to displacements. Most forces in this vector are zero.

We use lower-case, non-bold d^t for the column vector of $(D^t)^T$, and d^b for column vector of $(D^b)^T$, corresponding to the stresses on block B. After some rearrangement, the force vector $f^{loc} = K^{loc}u$ due to elastic forces produced by a block is

$$f^{loc} = K^{loc}u = Ewhl\left((d^t)^T u d^t + \frac{1}{6}h^2(d^b)^T u d^b\right)$$

Note that this equation implies that f is in the span of vectors d^t and d^b.

Let $\tilde{d}^t$, $\tilde{d}^b$ be the dual pair of vectors to d^t, d^b. Let the magnitudes of tensile and bending stresses be $|E(d^t)^T u| = \sigma^t$, $|E(d^b)^T u| = \sigma^b$; by taking dot products of both sides with the dual vectors $\tilde{d}^t$, $\tilde{d}^b$, we arrive at the equation, where we drop beam/cell subscripts:

$$wh\sigma^t = |f^t/l| = g^t, \quad \frac{1}{6}wh^3\sigma^b = |f^b/l| = g^b$$

Local optimization problem. The stress in the block, under our assumptions, reaches its maximal value at the top or bottom, where its magnitude is equal to $\sigma^t + h\sigma^b$. This leads to the critical stress constraint $\sigma^t + h\sigma^b = \sigma_0$. Using expressions for g^t and g^b above, which we keep fixed at the local step, this is equivalent to

$$\frac{g^t}{h} + \frac{6g^b}{h^3} = \sigma_0 a y$$

where we have switched to the variable $y = w/a$ introduced in (7), where a is the corresponding cell triangle height. Without loss of generality, we assume σ_0 to be 1, which can be achieved by renormalizing all forces to be one. The complete local problem in variables h_i^c, w_i^c, $i = 1, 2, 3$ is:

$$\min_{h^c, y^c} V(h^c, y^c) \quad \text{s.t.} \quad \frac{g_i^t}{h_i^c} + \frac{6g_i^b}{(h_i^c)^3} = \sigma_0 y_i^c a_i$$

$$0 \le h_i^c \le h_{max}, \quad y_i^c \ge 0, \quad \text{for } i = 1, 2, 3 \qquad (15)$$

$$y_1^c + y_2^c + y_3^c \le 1,$$

By eliminating the stresses, *we arrive at a single constraint per block* relating w and h, which we express as follows:

$$y = (6g^b z^2 + g^t z)/a \qquad (16)$$

where $z = h^{-1}$, the new variable we introduce to simplify the expressions. This allows us to eliminate all variables w_i^c from the local optimization problem, leaving only three variables z_i^c, with constraints $0 \le z_{min} \le z_i^c$, $i = 1, 2, 3$, and $z_{min} = (h_{max})^{-1}$.

We say that a cell is *filled* if the equality $y_1^c + y_2^c + y_3^c = 1$ is satisfied, i.e. the blocks completely fill the cell.

Without loss of generality, we assume that for the solution $z_1 \le z_2 \le z_3$; in practice, 6 problems corresponding to 6 permutations of $(1, 2, 3)$ need to be solved and minimal solution picked.

PROPOSITION 1. *The function $V(y^c)$ is a concave function of y_i. As a consequence, its minima are reached on the boundary of the constraint domain; specifically, it is reached at one of the five types of configurations:*

(1) *all three blocks have maximal thickness: $z_i^c = z_{min}$, $i = 1, 2, 3$;*
(2) *the cell is filled, i.e. $y_1^c + y_2^c + y_3^c = 1$, and no inequality constraint reaches equality;*
(3) *the cell is filled, and two thicker beams have equal thickness, $z_1^c = z_2^c$;*
(4) *the cell is filled, and two thinner beams have equal thickness, $z_2^c = z_3^c$;*
(5) *the cell is filled, and the thickest beam has maximal thickness $z_1^c = z_{min}$*

In the first case, the solution is completely determined. In the second case, there are four possibilities: no inequality constraint is active (a 2-variable unconstrained optimization problem needs to be solved, e.g., parametrized by z_1^c, z_2^c); the other three cases define one-parametric families of solutions, and one-dimensional unconstrained optimization needs to be performed to find exact values, as we explain below. These families can be parametrized by, e.g., $z_3^c = (h_3^c)^{-1}$, with the values of the remaining z_i^c and y_i^c determined from the active constraints. The proposition is proved in the appendix.

This behavior of V is in stark contrast to the low-volume formulation ignoring common areas of beam-like parts of the structure: one can see that in three cases out of four, it creates a completely filled cell.

Solving the optimization problem. Proposition 1 leads to an efficient algorithm for the local step.

Observe that the constraint $y_1^c + y_2^c + y_3^c = 1$ has the form

$$\sum_i g_i^t z_i^c + 6g_i^b (z_i^c)^2 = 1, \qquad (17)$$

i.e., it is quadratic in z_i. This allows us to reduce the problem to a set of unconstrained optimization problems in one or two variables.

(1) Compute g_i^b, g_i^t, $i = 1, 2, 3$, for current displacements.
(2) Evaluate $V(z)$, for the case 1 solution with $z_i^c = z_{min}$.
(3) For each permutation of $(1, 2, 3)$ solve three one-dimensional optimization problems, minimizing $V(z^c)$, for each of the cases 3-5, and the two-dimensional problem for case 2 of proposition Prop 1. In each case 3-5, substitute the active constraint for z_i^c into (17), yielding a quadratic equation in two remaining free variables, one of which is z_3^c. Solve it to express the other variable in terms of z_3^c, and solve a one dimensional optimization problem for $V(z_3^c)$. This yields a set of *solution candidates*; the minimal solution is guaranteed to belong to it.
(4) Pick the minimal solution from the set of solutions obtained for all possible permutations and cases on the previous step.
(5) Update w_i^c using formula $w_i^c = (6g_i^b z_i^c + g_i^t z_i^c)$, and recompute the global stiffness matrix K.

The convergence behavior of the method is considered in Section 8.

Handling polygonal cells and postprocessing. There are several factors not considered in the solution method above: (1) possible inconsistency of thickness values across diagonal edges inside triangulated polygonal cells; (2) the coherence of block widths and thicknesses along the edge lines of the quad mesh, approximating the optimized stress lines. While jumps in thickness/width along these lines do not affect the stresses in our simplified model, in practice, these are likely to lead to localized stress concentrations close to jumps, and they are aesthetically objectionable. (3) stress values may slightly exceed the maximal stress after a final global step.

We experimentally observe that many of the candidate solutions have close values, especially in areas with no predominant stress direction.

We address (1) primarily in the process of optimization, at step 4, we pick a minimal candidate solution with lowest block thickness on the diagonal, which may not be the most optimal one, as long as it does not deviate above a threshold. Once the optimization is complete, for each subcell of a polygonal cell we increase the lowest block thickness to the maximal minimal thickness over the whole cell. In addition, for each cell, we store a number of candidate solutions with the smallest volumes.

We address (2) in a post-processing step using stored candidate solutions: for each non-diagonal edge of a cell, we find its continuation edges along quad mesh edge line in both directions, and choose the candidate solution closest in width to the average of the previous and next edge widths along the edge line.

To address (3), we find all blocks with stress exceeding $\sigma_0 = 1$, and increase their thickness and width, while maintaining constraints, to decrease the stress to the bound. This process is repeated iteratively until convergence. We note that all additional steps are designed to ensure that the final result satisfies stress constraints: in all cases, we never decrease the amount of material in cells, so while the resulting solution may be suboptimal, it always satisfies stress constraints. In practice, the effect of these alterations on the resulting weight is small.
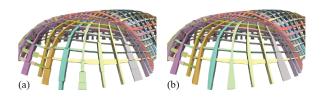
Fig. 11. Inflation: (a) Each block is meshed independently, leading to visible artifact; (b) An entire stream of edges is meshed to produce a smoother result

Inflation. Once we have performed the weight optimization, we have one value of thickness and one value of width for each half edge of the optimized polygonal mesh. If we simply extrude the solid block that matches thickness and width for each half edge cell we end up in the situation illustrated in Figure 11.a, where there are visible discontinuities between adjacent blocks, causing possible structural discontinuities. Instead, for each continuous stream of quad edges, we generate a unique solid block that interpolates thickness and width along its length (Fig. 11.b). In detail, given a sequence of aligned edges, we first derive a thickness value for each vertex by averaging the thickness from its adjacent half edges. Similarly, we interpolate widths, but this time we derive two different values for each vertex, one for each side of the sequence. We then define a tangent vector for each vertex as the cross product between its normal and its direction along the edge sequence (obtained by averaging the direction of the two incident edges). Then, having defined a proper reference frame, a thickness, and a width for each vertex, we have all the information to extrude a proper volumetric block. We perform a boolean operation to merge all the blocks together to a manifold watertight mesh using the approach of [Zhou et al. 2016].

8 EVALUATION

Topology optimization. To validate our approach vs. a general-purpose topology optimization method, we solve a similar problem with topology optimization code [Aage et al. 2015] by restricting the volume of the material to a cylinder of fixed small thickness, and choosing the volume grid resolution to be half of the cylinder thickness, leaving little room for shell shape variation. We observe that for small target volume fractions, as expected, structures emerging in topology optimization are similar to the beam structures we construct (Figure 12), with similar volume fractions. For a large volume fraction, the topology optimization method results in variable-thickness shells, but in this case, due to severe constraints on the thickness of the shell, this does not make a significant difference. Default parameters were used in [Aage et al. 2015].

Fig. 12. a) cylinder beam structure obtained using topology optimization with a target volume of 0.375; b) structure obtained using our method with a maximum thickness of 0.05 and a minimum thickness of 0.04.

Figure 13 shows the results of SIMP topology optimization vs. our method, with compliance as a function of the volume fraction. We observe similar behaviors for both methods. We note that in our case we need to choose the beam spacing parameter: when this is chosen too coarse, the performance will deteriorate.
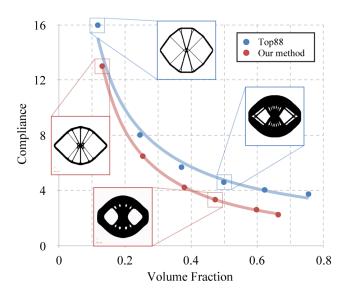

Fig. 13. Volume fraction vs. compliance energy for a standard example, a cantilever beam, SIMP topology optimization vs. our method.
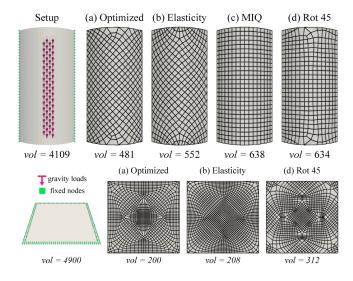

Fig. 14. Comparison of volumes obtained using different fields for the shell structure. Images (a-d) show the quad-mesh obtained with the different fields: (a) optimized stress directions from solving Eq. 14, (b) stress directions from solving elasticity, (c) MIQ field constructed using the smoothing method of [Bommes et al. 2009], and (d) constructed rotating (a) by 45 degrees.

The role of beam direction. In Figure 14, we explore the dependence of the role of beam direction in structure optimality, by comparing structure volume for several fields, in addition to our optimized field (Eq. 14). As a "worst-case" baseline we use the cross-field at a maximal distance from the original field (d); as one can see, the field makes a significant difference when it is very far away from the optimal directions, i.e., the choice of directions matters. Similarly, the curvature field (c), unrelated to stress directions, produces relatively high values of the volume. On the other hand, the difference between the optimized field and the stress field (a and b), while present, is relatively minor. This justifies the idea to use, as in, e.g., [Li et al. 2017], the elasticity stress field instead of the optimized field. The former has the additional advantage of better performance and higher smoothness.

Convergence and dependence on the starting point. We have observed that our algorithm almost invariably converges in several iterations, and yields the expected behavior of solutions in the extreme cases (ribs in the case of bending-dominant shells, and wide-and-thin beams in high-tension/low-bending areas.

The plots show the volumes at each iteration for a basic and more complex problem. Note that sometimes the optimal value is approached from below: the local step overshoots the volume reduction and the stress exceeds the maximal allowed level. Nevertheless, the method recovers reliably.
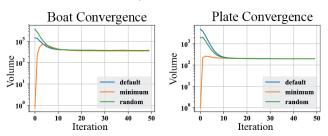

Fig. 15. Left: Volume convergence for our method, for the boat model, using different starting points. Right: similar plots for the bending plate.

We also compare our method to two general-purpose constrained optimization methods, SLSQP [Kraft 1988] and Ipopt, a barrier interior point method [Byrd et al. 2000]. In this setup, we used an approximation of the beams volume that is smoother (it uses average instead of *max*) and simple lower and upper bounds on the width and thickness. As a starting point, we have used the solution of the convex problem with volume ignoring the overlaps. Somewhat surprisingly, these methods were not able to change this initial solution by much after a few hundred iterations; although moving in the right direction, in terms of values, it may differ by a factor up to two from the optimal solution.

While the SLSQP solutions exhibited oscillatory behavior, alternating decreasing the functional with decreasing constraints violations, the interior point method solutions mostly stayed closed to the initial. Figure 16 shows comparative results with Ipopt for a small cantilever test case, we observe that Ipopt converges to a volume almost an order of magnitude larger. When Ipopt is initialized with the solution of the convex problem with simplified volume functional (green), the optimization fails to find a better solution. Using

a different initialization (orange: maximum width and thickness) does not provide better results. In contrast, our method converges to a much better solution in only a few iterations.
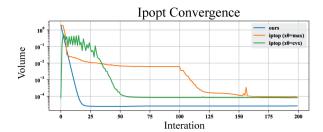

Fig. 16. Volume vs. iteration step for a small cantilever example (408 beams) using Ipopt vs. our method.

Effects of constraints on structure parameters. Figure 17 shows the effect of increasing maximal allowable thickness in a bending scenario, with the structure moving from fully solid, to a structure of narrow but tall beams (if the bound is increased to infinity, in principle, any bending force can be realized by a zero-volume infinitely thin rib).
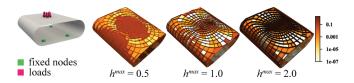

Fig. 17. In a bending dominated structure, changing the maximal allowed thickness from small to large causes the results to change from a solid plate to a rib-like structure.

Similarly, Figure 18 shows the effect of increasing *minimal* thickness in a *tensile* scenario. In this case, tall beams appear when increasing the lower bound because widths decrease to compensate for the increase of thickness. The usage of beams in tensile scenarios, while common, is often a consequence of constraints on minimum element size and are sub-optimal in the absence of these constraints. On the torsion cylinder experiment, the effect of using a minimal thickness of 0.04 vs. 0.00 increases the volume by 60%.
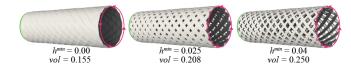

Fig. 18. In a tensile dominated structure, changing the thickness lower bound from small to large causes the results to change from a solid plate to a rib-like structure.

Relation to related work. A direct apples-to-apples comparison of different methods for optimization for shells is extremely difficult for a number of reasons, most importantly, because of different models used (all approaches use a variation of a beam model, and the specific choice has a significant impact on stress estimation). Another important reason includes a strong dependence of the results on the maximal width/thickness/aspect ratio constraints. We summarize qualitative differences from the most closely related works [Kilian et al. 2017] and [Li et al. 2017].

The key difference from [Kilian et al. 2017] is that it changes the shape of the surface, focuses on the case when bending forces can be neglected, and uses the narrow-beam volume approximation. This may be appropriate for targeted architectural applications but different types of solutions, produced by our method, may be more optimal when these can be practically manufactured. In comparison, we deal with a shell of fixed surface shape, take bending forces into account and use a more precise volume approximation, which leads to a non-convex problem.

[Li et al. 2017] takes the approach closer to ours, in that it constructs a quadrangulation following a field to determine beam directions and takes bending into account in the elasticity model. However, a narrow-beam approximation for the volume is used, and rather than using an optimized stress field as we do, the stress field of the non-optimized shell is used instead. In some cases, the optimized field provides an advantage, although the results are typically close as Figure 14 demonstrates. More importantly, the volume approximation has a major effect as shown in Figure 19, where we use one of the models we share with [Li et al. 2017]. In this case, the simpler volume approximation can increase the volume used by up to 44%. On the other hand, [Li et al. 2017] introduces I-beam optimization of beam cross-sections which we have not implemented, and may yield a substantial additional benefit. This technique can be easily combined with ours. Finally, [Li et al. 2017] does additional optimization of discrete beam directions, which can also be added to our method.
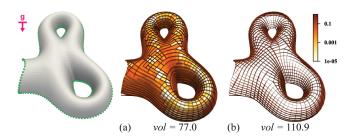

Fig. 19. Optimization results using different volume formula: (a) exact volume, (b) approximated convex volume.

Experiments. We have printed several simple structures to validate our optimization experimentally (Figures 20, 21, 22). Due to the highly approximate nature of the physical model used, we did not attempt a quantitative match to the simulated values, but we did closely match the values of the printed models. The comparison in all cases is between an optimized model and a uniform-thickness

model of the same weight. Observed displacements in all cases differed by a factor more than 3, suggesting a similar difference in stress.
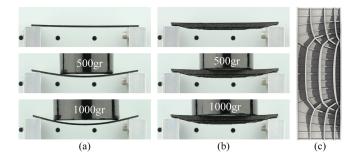

Fig. 20. (a) shelf based on original model (without optimization); (b) shelf printed from the optimized model; (c) optimized model.
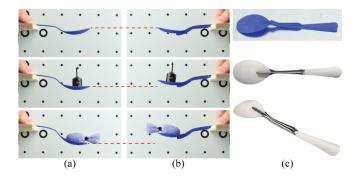

Fig. 21. (a) spoon based on original model (without optimization); (b) spoon printed from the optimized model; (c) optimized model.

Fig. 22. (a) leaf based on original model (without optimization); (b) leaf printed from the optimized model; (c) experiment setup; (d) optimized model.

Finally, Figure 24 shows a set of optimized shells obtained for a variety of shapes using our method; In all cases we have preserved a minimal width/thickness beam to indicate the mesh edges, but the load is carried by a relatively small number of beams; with shell shape constraints we found that unless the thickness bound is set

to very low values, even in tension areas ribs tend to appear. This is consistent with the observation that with no thickness, the load carried by bending forces is maximized, if the goal is to reduce the volume.

Fig. 23. Set of 3d printed models and a quarter (for scale).

	d(mm)	$|F|$	h	h^s	k	s	$t_{\text{solve}}(s)$
Aquadom	85.60	7742	0.5	0.005	100	0.2	72.330
Beetle	169.01	7558	1.2	0.012	50	0.5	35.999
Boat	92.60	9084	1.0	0.05	100	0.2	33.067
Botanic	42.59	2152	0.5	0.01	100	0.5	35.586
Bucket	21.57	7860	0.3	0.03	50	0.5	45.744
Bunny	106.00	7471	2.0	0.9	100	0.25	22.291
Duct	460.58	6932	1.0	0.01	100	0.2	69.593
Leaf	99.24	2980	2.0	0.9	46	0.5	1.954
Shelf	88.54	2400	4.0	0.5	60	0.5	1.663
Spoon	133.11	6528	4.0	0.9	29	0.5	4.129
Stevia	90.68	4840	2.0	0.9	50	0.5	23.941
Vase	69.64	4798	1.0	0.45	100	0.5	21.817

Table 1. Statistics for the 3D models in Figure 24 and Figure 1: the bounding box diagonal d (mm), the number of triangles $|F|$ in the input mesh, the maximum thickness h (mm) of the beams, the constant shell thickness h^s (mm), the number of iterations k and step-size s of the optimization solve, and the time t_{solve} it took to complete all iterations.

9 CONCLUSIONS AND FUTURE WORK

In this paper, we have described a way to approximate and efficiently solve the problem of minimizing the weight of a support structure for a shell. The proposed method separates the construction into three stages, with the first stage optimizing the field the beam directions must follow and creating a corresponding quad-dominant mesh, the second stage creating a cell structure with optimized shape parameters, and the third stage creating an actual realization.

This makes it particularly flexible and allows one to integrate a variety of additional user inputs and constraints, e.g., by modifying the field to change the truss directions, or by adding beams in the second stage to support a connection to a separate object. It is also

	$V^s(mm^3)$	$V^b(mm^3)$	$h_{eq}(mm)$	c_{eq}/c
Aquadom	16.989	90.335	0.032	1.601
Beetle	170.128	1287.227	0.103	5.739
Boat	189.997	418.539	0.160	7.099
Botanic	9.134	80.533	0.098	1.266
Bucket	15.028	8.325	0.047	26.924
Bunny	7270.428	1134.806	1.040	1.229
Duct	1075.645	19777.817	0.194	2.105
Leaf	2304.430	659.348	1.158	1.105
Shelf	1176.000	1386.550	1.090	7.252
Spoon	1544.960	326.733	1.090	18.621
Stevia	8329.664	2568.409	1.178	1.198
Vase	3505.556	492.212	1.026	1.953

Table 2. Performance for the 3D models in Figure 24. We show the ratio c_{eq}/c between the compliance c of our results and the compliance c_{eq} of a shell of constant thickness of the same weight. The fixed shell volume V^s, the support structure volume V^b, the thickness h_{eq} of the equivalent-weight constant thickness shell.

very efficient, with optimization converging in a few iterations, and quite consistently.

While we use a highly simplified model for cell mechanics, the overall approach admits replacing this model with a more advanced finite element formulation. In this case, it is likely that the local step would require numerical optimization; however, as long as the model for a cell stays low-parametric, one is likely to be able to solve it efficiently.

Limitations. Our work has two main limitations: first, the formulation for the field optimization still has restrictive low-volume and fixed-thickness assumptions. Based on our evaluation of field direction sensitivity of the final design, we do not view this as a major limitation. The second, more significant, limitation is the highly simplified model we used. If exact results are needed, this model can be used to quickly obtain an initial result, which can then be refined using a more advanced mechanical description of cells and shape optimization.

REFERENCES

Niels Aage, Erik Andreassen, and Boyan Stefanov Lazarov. 2015. Topology optimization using PETSc: An easy-to-use, fully parallel, open source topology optimization framework. *Structural and Multidisciplinary Optimization* 51, 3 (2015), 565–572.

Noam Aigerman and Yaron Lipman. 2015. Orbifold Tutte Embeddings. *ACM Trans. Graph.* 34, 6 (2015), 190:1–190:12.

Grégoire Allaire. 2002. *Shape Optimization by the Homogenization Method.* Number v. 146 in Applied Mathematical Sciences. Springer.

Grégoire Allaire and François Jouve. 2008. Minimum stress optimal design with the level set method. *Engineering analysis with boundary elements* 32, 11 (2008), 909–918.

MOSEK ApS. 2015. *The MOSEK optimization toolbox for MATLAB manual. Version 7.1 (Revision 28).*

Martin P. Bendsøe and Ole Sigmund. 2004. *Topology optimization: theory, methods, and applications.* Springer Berlin Heidelberg.

David Bommes, Henrik Zimmer, and Leif Kobbelt. 2009. Mixed-integer quadrangulation. *ACM Transactions On Graphics (TOG)* 28, 3 (2009), 77.

Richard H Byrd, Jean Charles Gilbert, and Jorge Nocedal. 2000. A trust region method based on interior point techniques for nonlinear programming. *Mathematical Programming* 89, 1 (2000), 149–185.

Marcel Campen, David Bommes, and Leif Kobbelt. 2015. Quantized global parametrization. *j-TOG* 34, 6 (2015), 192.

Hans-Christian Ebke, Patrick Schmidt, Marcel Campen, and Leif Kobbelt. 2016. Interactively Controlled Quad Remeshing of High Resolution 3D Models. *ACM Trans.*
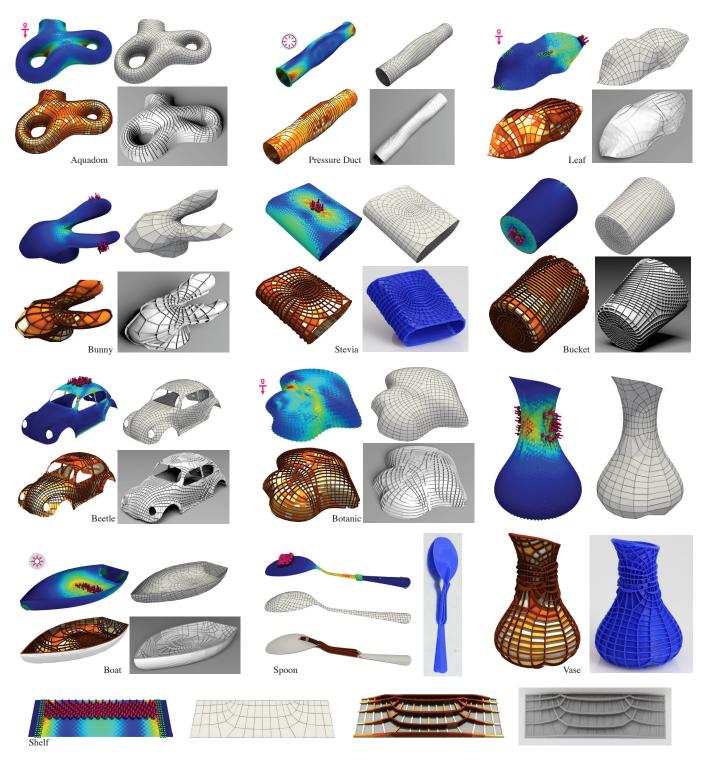
Fig. 24. Examples of structures obtained for a variety of shapes and loads. For each one, images show loads and initial stress distribution, quadrangulation, cell optimization (colored by thickness in logarithmic scale) and final geometry.

Eitan Grinspun, Yotam Gingold, Jason Reisman, and Denis Zorin. 2006. Computing discrete shape operators on general meshes. In *Computer Graphics Forum*, Vol. 25.

Wiley Online Library, 547–556.

Jeroen P Groen and Ole Sigmund. 2017. Homogenization-based topology optimization for high-resolution manufacturable microstructures. *Internat. J. Numer. Methods Engrg.* (2017).

W. S. Hemp. 1973. *Optimum structures.* Oxford, Clarendon Press.

Caigui Jiang, Chengcheng Tang, Hans-Peter Seidel, and Peter Wonka. 2017. Design and volume optimization of space structures. *ACM Transactions on Graphics* (2017).

Felix Kälberer, Matthias Nieser, and Konrad Polthier. 2007. QuadCover-Surface Parameterization using Branched Coverings. In *Computer Graphics Forum*, Vol. 26. Wiley Online Library, 375–384.

Martin Kilian, Davide Pellis, Johannes Wallner, and Helmut Pottmann. 2017. Material-minimizing forms and structures. *ACM Transactions on Graphics (TOG)* 36, 6 (2017), 173.

Felix Knöppel, Keenan Crane, Ulrich Pinkall, and Peter Schröder. 2015. Stripe Patterns on Surfaces. *j-TOG* 34, 4 (2015), 39:1–39:11.

Dieter Kraft. 1988. A software package for sequential quadratic programming. *Forschungsbericht- Deutsche Forschungs- und Versuchsanstalt fur Luft- und Raumfahrt* (1988).

Wei Li, Anzong Zheng, Lihua You, Xiaosong Yang, Jianjun Zhang, and Ligang Liu. 2017. Rib-reinforced Shell Structure. In *Computer Graphics Forum*, Vol. 36. Wiley Online Library, 15–27.

Yongqiang Li and Yong Chen. 2010. Beam structure optimization for additive manufacturing based on principal stress lines. In *Solid Freeform Fabrication Proceedings.* 666–678.

A.G.M Michell. 1904. The limits of economy of material in frame-structures. *The London, Edinburgh, and Dublin Philosophical Magazine and Journal of Science* 8, 47 (1904), 589–597.

David J Munk, Gareth A Vio, and Grant P Steven. 2015. Topology and shape optimization methods using evolutionary algorithms: a review. *Structural and Multidisciplinary Optimization* 52, 3 (2015), 613–631.

Ashish Myles, Nico Pietroni, and Denis Zorin. 2014a. Robust Field-aligned Global Parametrization. *ACM Trans. Graph.* 33, 4 (2014).

Ashish Myles, Nico Pietroni, and Denis Zorin. 2014b. Robust field-aligned global parametrization. *ACM Transactions on Graphics (TOG)* 33, 4 (2014), 135.

E. Oñate, F. Zárate, and F. Flores. 1994. A simple triangular element for thick and thin plate and shell analysis. *Internat. J. Numer. Methods Engrg.* 37 (1994), 2569.

Julian Panetta, Qingnan Zhou, Luigi Malomo, Nico Pietroni, Paolo Cignoni, and Denis Zorin. 2015. Elastic textures for additive fabrication. *ACM Transactions on Graphics (TOG)* 34, 4 (2015), 135.

Nico Pietroni, Davide Tonelli, Enrico Puppo, Maurizio Froli, Roberto Scopigno, and Paolo Cignoni. 2015. Statics aware grid shells. In *Computer Graphics Forum*, Vol. 34. Wiley Online Library, 627–641.

Nicolas Ray and Dmitry Sokolov. 2014. Robust polylines tracing for n-symmetry direction field on triangulated surfaces. *ACM Transactions on Graphics (TOG)* 33, 3 (2014), 30.

George IN Rozvany. 1976. *Optimal design of flexural systems: beams, grillages, slabs, plates and shells.* Elsevier.

George IN Rozvany. 2012. *Structural design via optimality criteria: the Prager approach to structural optimization.* Vol. 8. Springer Science & Business Media.

Ole Sigmund. 2001. A 99 line topology optimization code written in Matlab. *Structural and multidisciplinary optimization* 21, 2 (2001), 120–127.

Ole Sigmund, Niels Aage, and Erik Andreassen. 2016. On the (non-) optimality of Michell structures. *Structural and Multidisciplinary Optimization* 54, 2 (2016), 361–373.

Ole Sigmund and Kurt Maute. 2013. Topology optimization approaches. *Structural and Multidisciplinary Optimization* 48, 6 (2013), 1031–1055.

Jeffrey Smith, Jessica Hodgins, Irving Oppenheim, and Andrew Witkin. 2002. Creating models of truss structures with optimization. *ACM Trans. Graph.* 21, 3 (July 2002), 295–301.

Tomasz Sokół. 2011. A 99 line code for discretized Michell truss optimization written in Mathematica. *Structural and Multidisciplinary Optimization* 43, 2 (2011), 181–190.

Gilbert Strang and Robert V. Kohn. 1983. Hencky-Prandtl nets and constrained Michell trusses. *Computer Methods in Applied Mechanics and Engineering* 36, 2 (1983), 207–222.

Kam-Ming Mark Tam. 2015. *Principal stress line computation for discrete topology design.* Ph.D. Dissertation. Massachusetts Institute of Technology.

Kam-Ming Mark Tam, James R. Coleman, Nicholas W. Fine, and Caitlin T. Mueller. 2015. Stress line additive manufacturing (SLAM) for 2.5-D shells. *Proceedings of International Symposium on Shell and Spatial Structures.*

Jun Wu, Christian Dick, and Rüdiger Westermann. 2016. A System for High-Resolution Topology Optimization. *IEEE Transactions on Visualization and Computer Graphics* 22, 3 (March 2016), 1195–1208.

Tomás Zegard and Glaucio H. Paulino. 2014. GRAND — Ground structure based topology optimization for arbitrary 2D domains using MATLAB. *Structural and Multidisciplinary Optimization* 50, 5 (2014), 861–882.

Tomás Zegard and Glaucio H. Paulino. 2015. GRAND3 — Ground structure based topology optimization for arbitrary 3D domains using MATLAB. *Structural and*

Multidisciplinary Optimization 52, 6 (2015), 1161–1184.

Tomás Zegard and Glaucio H. Paulino. 2016. Bridging topology optimization and additive manufacturing. *Structural and Multidisciplinary Optimization* 53, 1 (2016), 175–192.

Haiming Zhao, Weiwei Xu, Kun Zhou, Yin Yang, Xiaogang Jin, and Hongzhi Wu. 2017. Stress-Constrained Thickness Optimization for Shell Object Fabrication. In *Computer Graphics Forum*, Vol. 36. Wiley Online Library, 368–380.

Qingnan Zhou, Eitan Grinspun, Denis Zorin, and Alec Jacobson. 2016. Mesh Arrangements for Solid Geometry. *ACM Trans. Graph.* 35, 4, Article 39 (July 2016), 15 pages. DOI:https://doi.org/10.1145/2897824.2925901

A CONVEXITY OF TRUSS CONTINUUM OPTIMIZATION

Expressing the functional in terms of entries of the stress matrix, using $a = (\sigma_{11} + \sigma_{22})/2$, $b = (\sigma_{11} - \sigma_{22})/2$, and $c = \sigma_{12}$, we obtain

$$|\lambda_1(\sigma)| + |\lambda_2(\sigma)| = 2\max(a, \sqrt{b^2 + c^2}) \tag{18}$$

which verifies convexity of the energy.

B DUAL OF THE CONTINUUM SHELL PROBLEM

This derivation follows [Strang and Kohn 1983], which we include here for completeness.

$$L(\sigma, \mathbf{u}) = \frac{E}{\sigma_0} \int_\Omega |\lambda_1(\sigma)| + |\lambda_2(\sigma)| dA + \int_\Omega \mathbf{u}^T \mathrm{div}\sigma dA - \int_\Omega \mathbf{f}^T \mu dA.$$

Integrating by parts, and assuming either free boundary $\partial_n \mathbf{u} = 0$ or fixed boundary $\mathbf{u} = 0$, we obtain

$$L(\sigma, \mathbf{u}) = \frac{E}{\sigma_0} \int_\Omega |\lambda_1(\sigma)| + |\lambda_2(\sigma)| dA - \int_\Omega \varepsilon(\mathbf{u}) : \sigma dA - \int_\Omega \mathbf{f}^T \mathbf{u} dA.$$

To obtain the dual we need to minimize over all possible σ in a coordinate system aligned with ε the expression

$$\frac{E}{\sigma_0}(|\lambda_1(\sigma)| + |\lambda_2(\sigma)|) - \lambda_1(\varepsilon)\sigma_{11} - \lambda_2(\varepsilon)\sigma_{22}.$$

The minimum of this expression is $-\infty$, if $|\lambda_i(\varepsilon)| > 1$, for either $i = 1$ or $i = 2$; otherwise, it is zero; this leads to the dual problem (10).

C PROOF OF THE PROPERTIES OF $V(z)$.

We drop the cell superscript c in this proof. We assume that $z_1 \leq z_2 \leq z_3$. By the constraints of the problem, $y_1 + y_2 + y_3 \leq 1$, $0 < z_{min} \leq z_i$.

$V(y, h)$ (1) is a quadratic function of y_i and linear in h_i; once we express it in terms of z_i, to eliminate the constraint between h_i and z_i, it becomes a cubic function of z_i, with Hessian

$$H(z) = \begin{bmatrix} A & -k_1 g_2^b & -k_1 g_3^b \\ -k_1 g_2^b & B & -k_2 g_3^b \\ -k_1 g_3^b & -k_2 g_3^b & -1/2 g_3^b \left(g_3^t + 3k_3\right) \end{bmatrix}$$

where $k_i = g_i^t + 2g_i^b z_i = dw_i/dz_i$, $B = -1/2 g_2^b \left(g_2^t + 3k_2 + 2g_3^t + 2k_3\right)$ and $A = -1/2 g_1^b \left(g_1^t + 3k_1 + 2g_2^t + 2k_2 + 2g_3^t + 2k_3\right)$.

A direct evaluation shows that $v^T H(z)v$ evaluated for $v = [1, 0, 0]$ is negative for positive z_i and $g_1^b \neq 0$. Similar is true for $v = [0, 1, 0]$ and $v = [0, 0, 1]$. We conclude if $g_i^b \neq 0$ for some i, any critical point in the interior of the domain is a maximum or a saddle, so there are

no minima in the interior. If all g_i^b are zero, the volume is a linear function of z_i, and the optimum is also on the boundary.

The constraint $y_1 + y_2 + y_3 \leq 1$ defines, if $g_b^i \neq 0$ for some i a quadratic surface in z_i coordinates, and the constraints $z_1 \leq z_2$, $z_2 \leq z_3$, $z_1 \geq z_{min}$ define 3 halfspaces. Their intersection is a tetrahedron with a curved face on the ellipsoid. The faces of the feasible domain correspond to one of the inequality constraints becoming an equality. Similarly, by a direct calculation, substituting either $z_1 = z_{min}$, $z_2 = z_1$ or $z_2 = z_3$ into $V(z)$ and computing 2 Hessians, we observe that these are not positive definite, hence there can be no solution on faces corresponding to the linear constraint. Finally, the same fact holds for pairs of constraints that define edges of the constraint domain, e.g., $z_1 = z_{min}$ and $z_2 = z_1$. We conclude that either the solution is on the face corresponding to the constraint $y_1 + y_2 + y_3 = 1$ or at the only vertex not on this face of the feasible domain, $z_i = z_{min}$, $i = 1, 2, 3$ (case 1 of the proposition). If the minimum satisfies $y_1 + y_2 + y_3 = 1$, it is either in the interior (case 2), or on one of the three edges of the boundary of that face (cases 3-5).

D DISCRETE BENDING STRAIN FOR BEAMS

The common normal $\mathbf{n}_i$ at i is defined as

$$\mathbf{n}_i = \sum_{\ell \in N(i)} \mathbf{e}_{i\ell} \times \mathbf{e}_{i\, next(\ell)}$$

where $next(\ell)$ is the edge following ℓ in CCW order around i.

At each vertex, we define a normal $\mathbf{n}_i$, as the average of cross-products of pairs of incident edges. For an edge $\mathbf{e}_{il}$, incident at a vertex i, let $\mathbf{e}_{im}$ be the next CCW edge, and $\mathbf{e}_{ip}$ be the previous edge. We define

$$\mathbf{q}_{lm} = \mathbf{e}_{il} \times \mathbf{e}_{im}$$

the (unscaled) normal to the triangle formed by i, l, m. Then $\mathbf{n}_i = \sum_{l,m \in N(i)} \mathbf{q}_{lm}$, and $\hat{\mathbf{n}}_i = \mathbf{n}_i / |\mathbf{n}_i|$.

We express the bending strain in the form $D_{ij}^b u$, where u is the vector of all vertex displacements. Define $\Delta \mathbf{e}_{ij} = \mathbf{u}_j - \mathbf{u}_i$. Then $\Delta \mathbf{q}_{lm} = \Delta \mathbf{e}_{il} \times \mathbf{e}_{im} + \mathbf{e}_{il} \times \Delta \mathbf{e}_{im}$. The part of $\Delta \mathbf{q}_{lm}$ affecting $\Delta \hat{\mathbf{n}}_i$ is the part perpendicular to $\hat{\mathbf{n}}_i$:

$\Delta q_{lm}^\perp = (I - \hat{\mathbf{n}}_i \hat{\mathbf{n}}_i^T) \Delta \mathbf{q}_{lm} = P_i \Delta \mathbf{q}_{lm}$, where P_i is the matrix $(I - \hat{\mathbf{n}}_i \hat{\mathbf{n}}_i^T)$. By substitution into the expression for n we get:

$$\Delta \hat{\mathbf{n}}_i = \frac{1}{|\mathbf{n}_i|} P_i \sum_{l \in N(i)} g_l \times (\mathbf{u}_l - \mathbf{u}_i)$$

where g_l is defined as follows:

- $g_l = \mathbf{e}_{ip} - \mathbf{e}_{im}$, if both p, m are in $N(i)$, i.e. $\mathbf{e}_{il}$ is not on the boundary.
- $g_l = \mathbf{e}_{ip}$, if $m \notin N(i)$.
- $g_l = -\mathbf{e}_{im}$, if $p \notin N(i)$.

For a vector $\mathbf{a} = [a_x, a_y, a_z]$, let $R(a)$ be the infinitesimal rotation matrix about a: $\begin{pmatrix} 0 & -a_z & a_y \\ a_z & 0 & -a_x \\ -a_y & a_x & 0 \end{pmatrix}$.

Then

$$\Delta \hat{\mathbf{n}}_i = \sum_{l \in N(i)} M_l^i (\mathbf{u}_l - \mathbf{u}_i)$$

where $M_l^i = \frac{1}{|\mathbf{n}_i|} P_i R(\mathbf{g}_l)$ is a 3×3 matrix.

$$\varepsilon^b[ij] = h \left(\sum_{l \in N(j)} (\mathbf{d}_{ji}^l)^T (\mathbf{u}_l - \mathbf{u}_j) + \sum_{l \in N(i)} (\mathbf{d}_{ij}^l)^T (\mathbf{u}_l - \mathbf{u}_i) \right)$$

where $\mathbf{d}_{ij}^l = -(M_l^i)^T \hat{\mathbf{e}}_{ij} / l_{ij}$, a vector of length 3. From this expression, we can immediately obtain D_{ij}.